ELSEVIER

Mechanics of Materials 32 (2000) 149–159

MECHANICS OF MATERIALS

www.elsevier.com/locate/mechmat

An investigation of the heat generated during cyclic loading of two glassy polymers. Part II: Thermal analysis

D. Rittel *, Y. Rabin

Faculty of Mechanical Engineering, Technion – Israel Institute of Technology, Technion City, Haifa 32000, Israel

Received 11 May 1999

Abstract

This paper presents the thermal analysis of cyclic compression experiments which were carried out on commercial PC and PMMA cylindrical specimens. The thermal problem is solved numerically (finite element). Uniform internal heat generation is assessed from the experimental evolution of the hysteretic energy rate throughout the experiment. The results show a very good agreement between the calculated and the measured temperatures. The temperature peak which characterized the PC specimens and the continuously rising temperature of the PMMA cylinders are very well reproduced using simple assumptions of uniform heat generation and a constant ratio of the thermal to mechanical power conversion ($\beta = 0.5$). The mathematical solution provides information on the temperature distribution and its dependence on the boundary conditions (insulation of the specimen from the platens). These results are discussed with respect to surface temperature sensing of polymeric materials.

Keywords: Glassy polymer; PMMA; PC; Thermomechanical coupling; Hysteretic heating; Cyclic loading; Numerical solution; Thermal analysis

1. Introduction

In the first part of this work (Rittel, 2000), we presented results on the hysteretic heating of commercial PMMA and PC. Cylindrical specimens were tested in compression at relatively high stress amplitudes (scaled with respect to the yield strength). While the cylinders were virtually identical and were tested in similar conditions, a marked difference in their thermal response was observed. Specifically, the PC specimens exhibited a high temperature peak during the initial part of the loading, followed by a plateau phase and subsequent rise again, towards final failure. By contrast, the temperature of the PMMA kept increasing until final failure. An additional difference was observed in the failure modes of these materials: the PC cylinders failed by barreling, whereas the PMMA cylinders exhibited a localized bulging at failure.

One important conclusion was that the nature of the thermal process deserves further study to deepen our understanding of the consequences of hysteretic heating. It appears that two factors should be considered: the first is the extent of the thermomechanical coupling, which conditions the temperature changes. The second relates to the boundary conditions of the specific problem which

* Corresponding author. Tel.: +972-4-829-32-61; fax: +972-4-832-45-33.

E-mail address: rittel@dany.technion.ac.il (D. Rittel).

0167-6636/00/$ - see front matter
PII: S0167-6636(99)00052-6

determine, in turn, the temperature distribution and the resulting failure mode.

Consequently, we further investigate the conversion of mechanical into thermal energy for the specific experiments, which are described in the first part of this paper. The main idea is to obtain a *realistic approximation* of the temperature field within the specimen, given the evolution of the dissipated energy throughout the experiment. It is shown that the specific thermal response could be predicted, based on the general evolution of the dissipated energy throughout the experiment. Finally, conclusions are drawn regarding bulk vs. surface temperature measurements.

2. Theoretical background and numerical model

2.1. Theoretical background

The basic equations were developed in the first part of the paper and will only be briefly addressed here. The heat balance equation, including a heat generation term, is written as follows:

$$\beta \dot{W}_{\text{in}} + k\nabla^2 T = \rho c_{\text{E}} \dot{T}, \tag{1}$$

where k is the thermal conductivity, ρ the density, c_{E} the specific heat, T the temperature, W_{in} and β are addressed below.

The dissipated energy (per volume) is given by:

$$W_{\text{in}} = \Pi \sigma_0 \varepsilon_0 \sin\delta, \tag{2}$$

where σ_0 and ε_0 stand for the amplitude of the cyclic stress and strain, respectively. The value of $\sin\delta$ is obtained from the hysteresis loop formed by plotting the stress vs. strain. The rate of dissipated energy $\dot{W}_{\text{in}}$ is evaluated over one cycle. The factor β, which multiplies $\dot{W}_{\text{in}}$, expresses the ratio of the thermal to mechanical power (neglecting thermoelastic effects). While it has been established that this factor is both strain and strain-rate dependent (Mason et al., 1994; Rittel, 1999), we did not attempt to evaluate its varying value for cyclic loading of the investigated polymers. Rather, we assumed, as a first approximation, that β is constant. It should be noted that, for cyclically loaded copper tubes, Dillon (1966) showed that this ratio varied throughout the single cycle. In this sense, our constant value will be considered as an average value.

2.2. Numerical model

The specimen and the experimental setup are described schematically in Fig. 1. The cylindrical specimen is placed between two rigid platens. In the same figure, a two-dimensional sketch of the problem is shown. The analysis is two-dimensional and axially-symmetric. For the purpose of analysis, the following points in the specimen are defined: point 1 corresponds to the location of the core thermocouple; points 2–4 are located on the outer boundary of the specimen. Point 5 corresponds to the location of a second thermocouple, located close to the specimen–platen interface

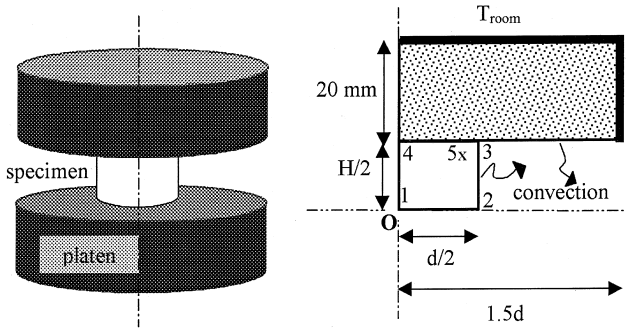

Fig. 1. Schematic representation of the experimental setup and the model for numerical analysis. Five representative points are selected. Point 1 is located at the center of the specimen, points 2–4 on the specimen boundaries. Point 5 is located 1 mm below the platen and 1 mm from the outer surface.

(about 1 mm below the platen and 1 mm from the outer surface). Such a thermocouple was used to assess the uniformity of the temperature in the specimen (see part I). The following thermal boundary conditions are assumed:

1. heat transfer by conduction between the specimen and the platens;
2. heat transfer by convection from the specimen outer surface to the surroundings;
3. heat transfer by convection from the platen exposed surface and the surroundings;
4. uniform initial temperature distribution;
5. a constant temperature at the far end of the platens from the specimen, equal to the initial temperature.

Internal heat generation was applied to the cylindrical specimen only. Two typical cases were numerically solved: the first consists of an ''insulated'' specimen for which the cylinder and the platens (without internal heat generation) are made of the same polymeric material. Polymeric platens have thermophysical properties which are similar to those of the ceramic platens which were inserted, in most experiments, between the specimen and the steel platens. In the second case, designated as the ''non-insulated'' case, the platens were assumed to be made of carbon steel. The model was discretized for finite element analysis and solution of Eq. (1) with the appropriate boundary conditions. The temperature distribution was solved using ANSYS (1994), which is a commercial finite element package. The setup was meshed with eight node axisymmetric thermal solid element (PLANE77). The experimentally determined evolution of the dissipated energy rate, $\dot{W}_{\mathrm{in}}(t)$, was applied as internal heat generation rate in the numerical model. $\dot{W}_{\mathrm{in}}(t)$ was assumed to be uniformly distributed in space. The ratio of the thermal to mechanical power (neglecting thermoelastic effects) was taken as a constant, $\beta = 0.5$. The various coefficients and material properties used in the calculations are detailed in Appendix A. The thermal conductivity of the investigated materials was assumed to be constant and uniform (Waterman, Ashby, 1991). By contrast, the specific heat of these materials was treated as temperature-dependent (Tadmor, 1979).

3. Results

3.1. Experimental

Fig. 2 shows characteristic temperature evolutions, as measured in the core of PC specimens. Each specimen was stressed at a different relative stress amplitude with respect to its yield strength. As expected, specimen D5, which was stressed near its yield strength, exhibits a marked temperature peak when compared with other specimens stressed at lower amplitudes. The corresponding hysteretic energy rates (per cycle) are plotted in Fig. 3. It can be seen from this figure that, in spite of the noticeable scatter in the results, the following tendency is observable: the higher the stress amplitude, the greater the number (cluster) of high energy points at the initial stage of the experiment. This is particularly remarkable when comparing the results of specimen D5 with those of D18 for example. The results obtained for two selected PMMA specimens are shown in Fig. 4. Here, the temperature increases monotonically until final failure. The corresponding dissipated strain energy per cycle is scattered in this case too. Nevertheless, the energy tends to increase with time. It is also noted that by contrast with PC, there is no cluster of high energy points for PMMA.

3.2. Numerical

3.2.1. Core temperatures

Comparison of experimental data and numerical solution of the core temperature is shown in Figs. 5 and 6 for PC (specimens D5 and D18) and PMMA (specimens D12 and D17), respectively. For these cases, the ''insulated'' model has been used. A very good agreement can be observed between the numerical and experimental results. This indicates that the calculations closely replicate the actual physical process.

3.2.2. Insulated vs. non-insulated case

Fig. 7 shows the core and near-surface temperatures calculated for the insulated and non-insulated cases. The influence of the absence of insulation is evident in the sense that it lowers the values of the temperature field. On the other

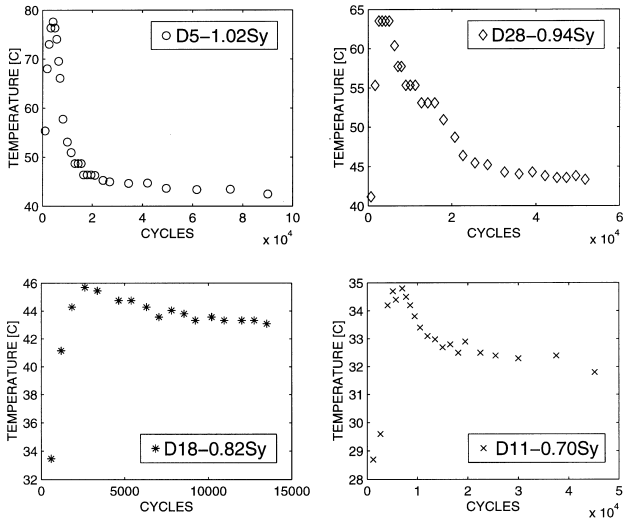

Fig. 2. Experimental results for the core temperature of insulated PC specimens (D5, D28, D18 and D11). The specimens were cyclically loaded at different relative amplitudes (with respect to yield strength, Sy). Note that the higher the amplitude, the better defined the thermal peak.

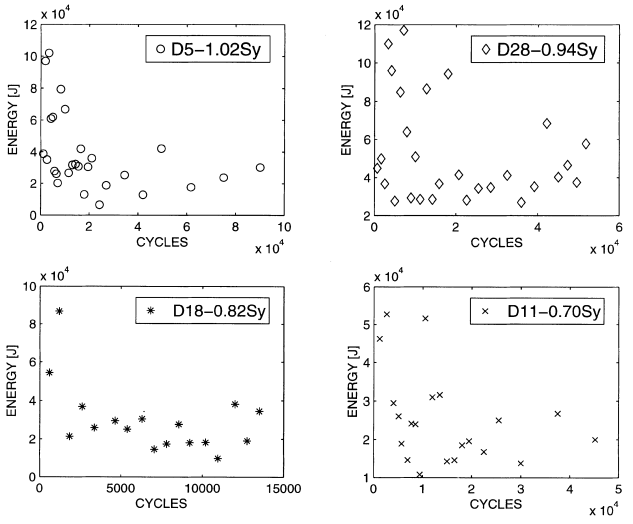

Fig. 3. Evolution of the hysteretic energy per unit volume per cycle, for the PC specimens shown in Fig. 2. High-energy points tend to cluster at the initial stages for specimens loaded at higher amplitude.

hand, the similarity in both cases is that the peak temperature is always found at the core, regardless of the applied boundary conditions. Here too, the present results corroborate results shown in the first part, in which the non-uniformity of the temperature field was investigated experimentally.

3.2.3. Temperature distribution within the specimen

For the analyses of the temperature field within the specimen cross-section, the following non-dimensional temperature is introduced:

$$\theta_i(t) = \frac{T_i(t) - T_\infty}{T_1(t) - T_\infty}, \tag{3}$$

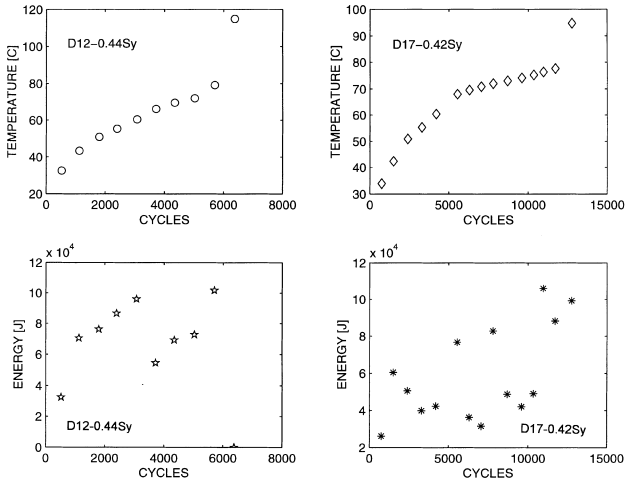

Fig. 4. Experimental results for the core temperature and the corresponding hysteretic energy per unit volume per cycle for insulated PMMA specimens (D12 and D17). The temperature increases steadily, and there is no clustering of high-energy points, as in the case of PC.

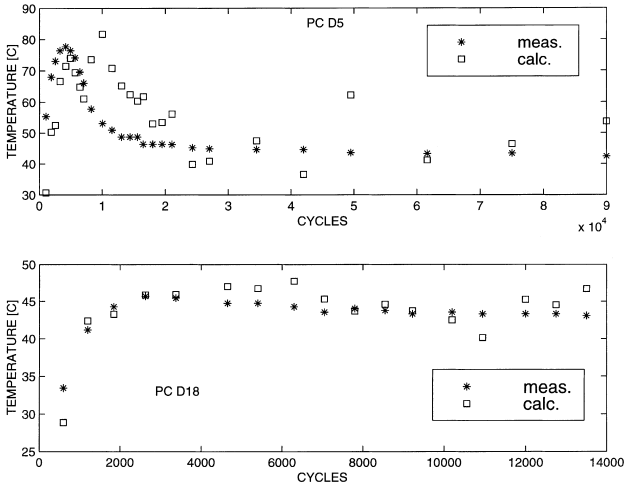

Fig. 5. Numerical and experimental results for the core temperature of PC, specimens D5 and D18. Note the very good agreement between the numerical and the experimental results.

where T_i is the temperature at a specified location, T_∞ the surroundings temperature, and T_1 is the core temperature. The non-dimensional temperature presented in Eq. (3) is an indicator of the uniformity of the temperature field within the cross-section. A value of 1 indicates high uniformity, while the value of 0 indicates maximal temperature differences.

Figs. 8 and 9 show typical time dependence of temperatures at the various locations specified in the insert of these figures, for PC and PMMA insulated specimens, respectively. Both figures show that θ_i is almost time- (or number of cycles)-independent. The value of θ_2 is close to 0.8, which indicates a 20% temperature variation in the radial direction, when compared with the maximal

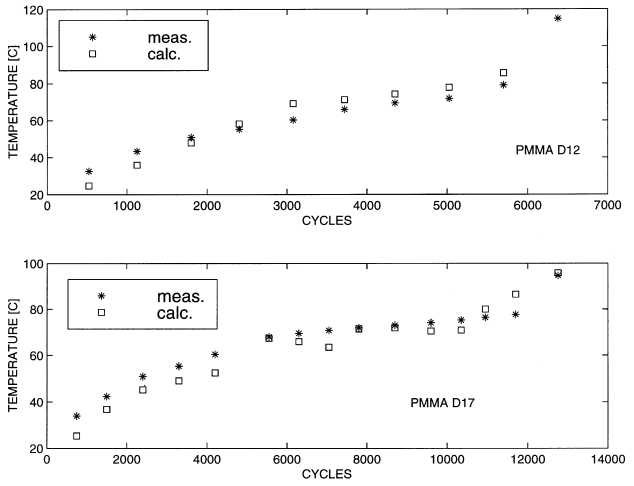

Fig. 6. Numerical and experimental results for the core temperature of PMMA specimens D12 and D17. Here too, agreement between the numerical and the experimental results is very good.

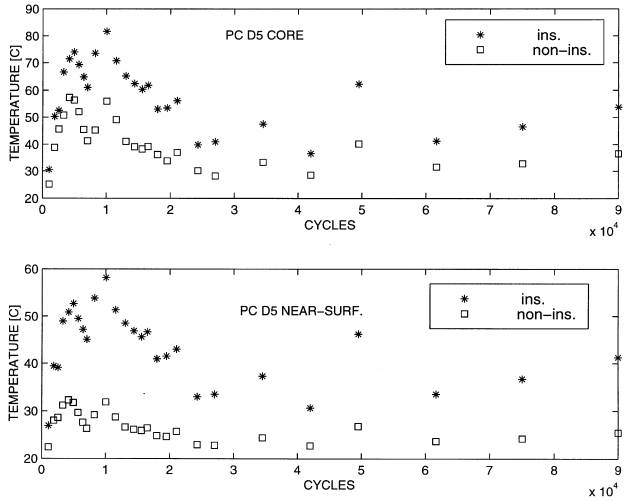

Fig. 7. Numerical results for the core (point 1) and the near surface (point 5) temperatures of PC specimen D5. Calculation was performed for the insulated (ins.) and non-insulated (non-ins.) case.

possible temperature difference. The observation of a significant radial temperature variation coincides with *Biot* number of the order of 1, where *Biot* number is a non-dimensional number representing the ratio of the thermal resistance to radial heat conduction and the thermal resistance to heat flow by convection to the surroundings:

$$Biot = \frac{hd}{k}, \tag{4}$$

where d is the specimen diameter. When evaluating the non-dimensional results presented in Figs. 8 and 9, one should bear in mind that the actual temperatures are changing with time, at any spe-

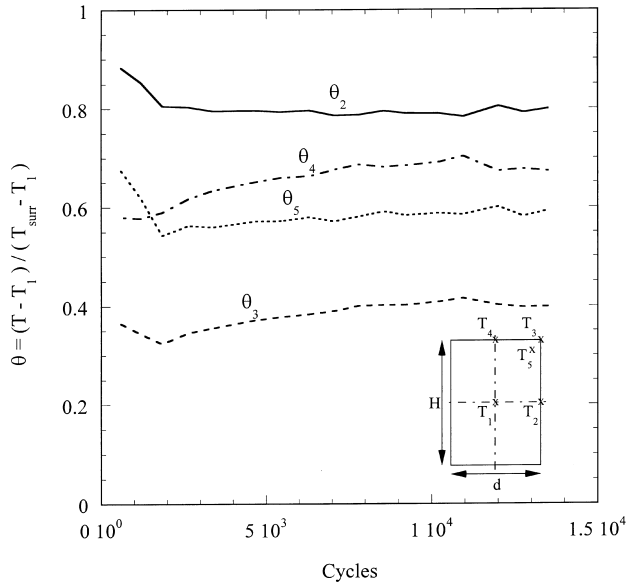

Fig. 8. Non-dimensional temperature evolution in an insulated model of a PC specimen (D18).

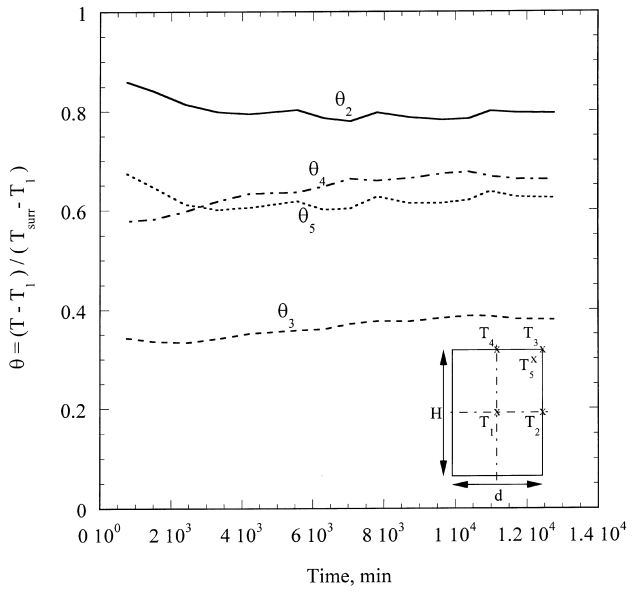

Fig. 9. Non-dimensional temperature evolution in an insulated model of a PMMA specimen (D17).

cific point within the specimen, as shown in the previous figures. However, these changes are proportional everywhere in the field in such a way that the non-dimensional temperatures representing this process remain almost constant.

Figs. 10 and 11 show the difference between the insulated and non-insulated models of the same PC specimen, as a result of the same heat generation history. The core temperature in both cases is essentially the same. However, the base

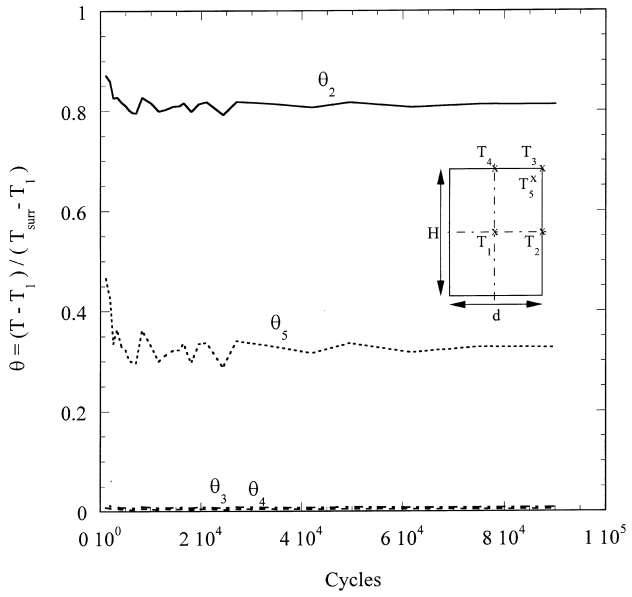

Fig. 10. Non-dimensional temperature evolution in a non-insulated model of a PC specimen (D5).

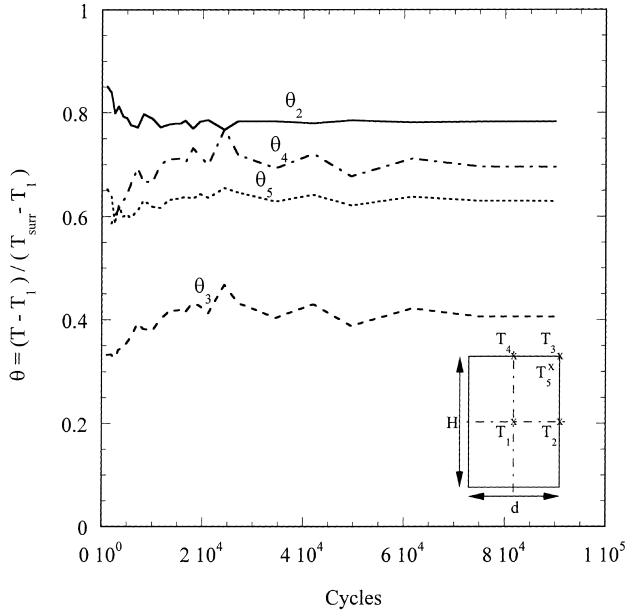

Fig. 11. Non-dimensional temperature evolution in an insulated model of a PC specimen (D5).

temperatures of the non-insulated model (θ_3 and θ_4) have almost not changed from their initial value, whereas the base temperatures in the insulated case vary in the range of 0.4–0.7. This indicates that the base temperature is dominated by the thermophysical properties and the heat

capacity of the platens in the non-insulated case. The temperature at 1 mm from the specimen base and surface, θ_5, is also influenced by the platens. Finally, the lower temperatures shown in Figs. 8–11 are found at the outer surface of the specimen, and in contact with the platen (point 3). This is expected since this point is exposed *both* to heat conduction to the platen and heat convection to the surroundings.

3.2.4. Possible implications for surface temperature sensing

Temperature measurement using thermocouples, as performed in this study, suffers from the disadvantage of collecting temperature data from one or more discrete locations. Another limitation is the possible heat conduction by the thermocouple, which may interfere with the readings. This difficulty can be overcome by using an infrared temperature measurement technique, which gives the surface temperature distribution with minimal interaction between the sensor and the sensed phenomenon (see e.g., Arruda et al., 1995; Trojanowski et al., 1997). Figs. 8–11 indicate significant temperature distribution in the radial direction, at any specific height of the specimen: the outer surface temperatures are about 20% lower than the temperature at the center of the specimen at its mid-height, and about 45% lower at the base of the specimen in an insulated model. This means that infrared temperature measurements of the surface may indicate only about one half of the actual temperature difference between the center of the specimen and its surface, when focussing on points in the vicinity of the specimen's base. This leads to the conclusion that infrared temperature measurements may be misleading when experimenting with cylindrical polymer specimens. Previous work on metals by Kapoor and Nemat-Nasser (1998) has raised a similar question about the accuracy of infrared sensing techniques. Therefore, it is highly suggested that infrared temperature measurements will be performed only in cases characterized by low *Biot* number, say $Biot < 0.1$.

4. Summary

The numerical study presented here shows that once the dissipated energy has been assessed, the temperature evolution and distribution can be calculated using simple assumptions, such as to match the experimental observations. For this purpose, we assumed spatial uniformity of the energy distribution. Likewise, a constant conversion ratio of mechanical into thermal power has been assumed. While the latter varies during the cycle, the value employed here was shown to yield satisfactory results with respect to the measured data. One could of course match an "optimal" function for $\beta(t)$ based on some parametric estimation technique. At this stage, however, a constant value of $\beta(t)$ is considered as fairly adequate to reproduce the salient experimental observations. It is also noted that such a low value for $\beta(t)$, of the order of 0.5, indicates that a non-negligible part of the hysteretic energy is actually stored through microstructural modifications. Similar observations were made by Salamatina et al. (1994). On the other hand, experimental effort should be dedicated to the determination of $\beta(t)$ to improve the predictive capability.

Another important outcome of this study concerns the distribution of hysteretic energy and the observed evolution of the core temperature. It appears that, even if the energy distribution suffers from inherent experimental scatter, it nevertheless indicates qualitatively the expectable temperature evolution. This observation stems from the fact that $\dot{W}_{\text{in}}$ and $\dot{T}$ are of the same order with respect to time. Therefore, the initial cluster of high energy points observed in PC specimens correlates with the observed (and calculated) temperature peak, in contrast with PMMA specimens.

Finally, the value of the temperature reached and its distribution within the specimen cross-section determine the attainment of a failure criterion, which is expected to rely on a critical temperature (see e.g., Dillon, 1976). Here again, the center of the specimen is the expected locus for the higher temperature, regardless of the boundary conditions. However, the calculations indicate that if the temperature of the specimen

is assessed using surface measurements (e.g., infrared), care should be exercised as to the location of the probed point(s) and the assessment of the maximal temperatures within the specimen.

5. Conclusions

The temperature distribution and evolution was calculated, using simple assumptions, and compared to experimental observations for cyclically loaded PC and PMMA.

- A very good agreement was found between the numerical and the experimental temperatures, using the hysteretic energy as an input, for the two materials.
- The center of the specimen is the expected and observed locus for the higher temperature, regardless of the boundary conditions.
- The calculations indicate that if the temperature of the specimen is assessed using surface measurements (e.g., infrared), care should be exercised as to the location of the probed point(s) and the assessment of the maximal temperatures within the specimen.

Acknowledgements

This research is supported by the Israel Science Foundation under grant no. 030-039. Dr. R. Levin's assistance is gratefully acknowledged. Y. Rabin acknowledges support of Stanley Imerman Memorial Academic Lectureship – USA. Useful discussions with Prof. A. Benatar (OSU) are acknowledged.

Appendix A

For all calculations, the initial and outer reference temperatures were taken as $T_{ref} = 293$ K. The convection heat transfer coefficient was assumed $h = 15$ W/m^2 K. The following material properties were used for the numerical calculations.

(a) *PMMA*. Density: 1199 kg/m^3, k (thermal conductivity): 0.2 W/m K and temperature dependent specific heat (Tadmor, 1979):

T (K)	C_p (J/kg K)
319	1440
349	1615
370	1760
390	2165
433	2240
462	2300

(b) *PC*. Density: 1199 kg/m^3, k (thermal conductivity): 0.2 W/m K and temperature-dependent specific heat (Tadmor, 1979):

T (K)	C_p (J/kg K)
331	1440
361	1494
380	1600
412	1788
442	2036
497	2127

(C) *Steel* (*platens*). Density: 7800 kg/m^3, k (thermal conductivity): 54 W/m K and specific heat (Holman, 1986): $C_p = 465$ J/kg K.

References

ANSYS, User's Manual, 1994. Swanson Analysis Systems Inc.

Arruda, E.M., Boyce, M.C., Jayachandran, A., 1995. Effects of strain rate, temperature and thermomechanical coupling on the finite strain deformation of glassy polymers. Mech. Mater. 19, 193–212.

Dillon, O.W., 1966. The heat generated during the torsional oscillations of copper tubes. Int. J. Solids Struct. 2, 181–204.

Dillon, O.W., 1976. Adiabatic heating as a cause of low cycle fatigue failure. Mech. Res. Commun. 3, 367–372.

Holman, J.P., 1986. Heat Transfer, sixth ed. McGraw-Hill, Kogakusha.

Kapoor, R., Nemat-Nasser, S., 1998. Determination of temperature rise during high strain rate deformation. Mech. Mater. 27, 1–12.

Mason, J.J., Rosakis, A.J., Ravichandran, G., 1994. On the strain and strain rate dependence of the fraction of plastic work converted into heat: an experimental study using high speed infrared detectors and the Kolsky bar. Mech. Mater. 17, 135–145.

Rittel, D., 1999. On the conversion of plastic work to heat during high strain rate deformation of glassy polymers. Mech. Mater. 31, 131–139.

Rittel, D., 2000. An investigation of the heat generated during cyclic loading of two glassy polymers. Part I. Experimental. Mech. Mater. 32, 131–147.

Salamatina, O.B., Höhne, G.W.H., Rudnev, S.N., Oleinik, E.F., 1994. Work, heat and stored energy in compressive plastic deformation of glassy polymers. Thermochim. Acta 247, 1–18.

Tadmor, Z., 1979. Principles of Polymer Processing. Wiley, New York.

Trojanowski, A., Ruiz, C., Harding, J., 1997. Thermomechanical properties of polymers at high rates of strain. J. Physique Coll. C 3, 447–452.

Waterman N., Ashby, M.F. (Eds.), 1991. Elsevier Materials Selector. Elsevier, London, p. 1510.